Hindawi
Journal of Sensors
Volume 2021, Article ID 6348347, 12 pages
https://doi.org/10.1155/2021/6348347

Research Article

Performance Analysis of Vibration Sensors for Closed-Loop Feedback Health Monitoring of Mechanical Equipment

Yue Xiao,[1] **Yan Li**,[2] **and Changbao Chu**[1]

[1]*School of Mechanical Engineering, Nanchang Institute of Technology, Nanchang Jiangxi 330099, China*
[2]*School of Information Engineering, Nanchang Institute of Technology, Nanchang Jiangxi 330099, China*

Correspondence should be addressed to Yue Xiao; xy@nit.edu.cn

Received 15 September 2021; Accepted 2 October 2021; Published 26 October 2021

Academic Editor: Guolong Shi

In this paper, we analyze the performance of mechanical equipment through a closed-loop feedback health monitoring vibration sensor, develop an OTDR optical signal reception and the processing module, and realize the reception, amplification, and filtering of the backscattered optical signal. In terms of vibration signal demodulation, the FPGA signal processing module was developed and debugged to realize the intermodulation with OTDR optical signal reception processing module and the preprocessing of the vibration data stream by taking advantage of the FPGA in parallel high-speed data stream processing. The objective function is constructed based on the dynamic data of the first four vertical frequencies of the modal recognition and the static data of the constant-load cable force of the inclined cable, and the third-order response surface method is applied to fit the response surface function of each correction target. The errors between the corrected FEM calculated values and the measured results are within 5%. The results were compared with the results of static and dynamic corrections, and the results showed that the joint static and dynamic corrections using the third-order response surface could obtain a finite element model that was more comprehensive and closer to the actual engineering response. A 180° feedback gain is set in the mass detection system to reduce the system's equivalent mass and increase the system resonant frequency. An inverse lock-in amplifier is used instead of a high-frequency bandpass filter to spectrally migrate the useful frequencies and better filter out noise interference. A thin-film microresonant pressure sensor, a cantilever beam microresonant gas sensor, and a microresonant biosensor were designed and developed using the micromachining process. A closed-loop feedback method was used to design a low-frequency detection system, a medium-frequency detection system, and a high-frequency feedback detection based on a phase-locked loop system, completed open-loop and closed-loop detection experiments of the intrinsic frequency of the sensor, through-pressure experiments of the pressure sensor, low and medium frequency gas-sensitive experiments of the gas sensor, and high-frequency detection experiments of the biosensor oxygen absorption/deoxygenation, and measured the mass of individual oxygen molecules.

1. Introduction

Microsensors, as an important part of MEMS systems, are a key part of the acquisition of external target signals and usually consist of a signal-sensitive element and a signal conversion element. Among them, the signal-sensitive element can sense the external signal changes and change accordingly, while the signal conversion element converts the physical change of the sensitive element into an electrical signal suitable for subsequent measurement and transmission. Compared with traditional sensors, microsensors are becoming smaller and more integrated and easy to achieve batch production, which is an important contribution to the miniaturization and intelligent development of the system [1]. Microsensors with different functions have been widely used in consumer electronics, artificial intelligence/robotics, smart wear, smart home, automotive industry, smart factory, etc. They play an important role in national economic and technological development and are an important pillar of modern information technology and have become an important research direction in MEMS systems at home and abroad [2]. The output signal of the microresonant

sensor is a frequency signal, which can be directly input to the signal processing module without conversion and is not easily distorted in long-distance transmission and detection, and this type of sensor has the advantages of small size, easy integration with the test circuit, and rapid response [3]. Resonant MEMS sensors, which use micron/nanometer-scale mechanical elements obtained by micromachining processes as resonators and are composed of other parts such as substrates or pressure membranes, are one of the important forms of microsensors. The main advantages of MEMS sensors are small size, lightweight, low power consumption, high reliability, high sensitivity, easy integration, etc. are the main force of microsensors, and are gradually replacing the traditional mechanical sensors, in almost all areas of research, whether it is consumer electronics, automotive industry, and even aerospace, machinery, chemical and pharmaceutical, and other fields. The working mechanism of this type of sensor is that the resonant oscillator undergoes regular changes in its intrinsic frequency when the target to be measured changes, and the detection of the external environment is achieved by detecting the amount of change in the intrinsic frequency. With the development of micromachining technology, the size of the sensor resonator is getting smaller and smaller, even to the nanometer level, and when the resonator has a higher resonant frequency, while the resonant sensor composed of the nanoscale resonator has a smaller air damping, its quality factor Q is higher, with higher sensitivity.

As the core component of the microresonant sensor, the resonator is mainly based on the anisotropic properties of silicon material, using micromachining technology to process the silicon substrate, and its structure can be summarized into four basic forms [4]. Film type, scraper conveyor with scraper chain and central groove as the traction mechanism and support mechanism, respectively, through the sprocket chain meshing action to achieve the operation of the whole equipment, is typical double chain traction flexural continuous. It is a typical double chain traction flexible continuous transport equipment. The chain drive system of the scraper conveyor is a closed continuous operation system, mainly composed of scraper chain, drive sprocket, central groove, and scraper. There is a complex movement and force relationship between each component. In the actual production process of a coal mine, the operating conditions of the scraper conveyor are very harsh, and the chain drive system has a long transmission distance, and the actual operation is affected by the bending and inclination of the working surface, the meshing polygon effect, and the factors of each component's material, wear, and corrosion, etc., but also bears the impact of external load impact and uneven load distribution and other variable load conditions, which directly leads to the key chain drive system. Parts' failure rate is high [5], damage serious, affecting the safe operation of the equipment. Thus, the main problems involved in the study of the safety and reliability of the chain drive system of heavy scraper conveyors in coal mines include the study of the force characteristics of the scraper chain, the monitoring of the operating condition, and the diagnosis and early warning of typical faults. Microsensors are the most successful and practical micromechanical devices, mainly including micropressure sensors and microacceleration sensors that use mechanical deformation of microdiaphragms to generate electrical signal output. With the further development of microelectronic processing technology, especially nanofabrication technology, sensor technology will also evolve from microsensors to nanosensors. The small size of these miniature sensors, the ability to perform many new functions, the ease of high-volume and high-precision production, the low cost per piece, and the ease of forming large-scale and multifunctional arrays make them well suited for automotive applications.

This paper is aimed at the demand of high quality and high-efficiency machining of complex thin-walled curved parts, targeting the lack of flexibility of traditional CNC machining machine tools, the defects of functional structure forming machining method, and the gap of result quality measurement method, and carries out the following researches from the technical details and feasibility of the integrated system of machining and inspection. First, to address the problem of motion flexibility of traditional CNC machine tools, we design and develop a multidegree-of-freedom industrial robotic arm and a special workpiece fixture and explore the trajectory planning method and offline programming control technology of the industrial robotic arm; second, to address the low stiffness defects of the robotic arm and the thin-walled characteristics of the part, we introduce a laser without macro cutting force to realize three-dimensional pattern manufacturing, study the multipulse laser etching process, and design a composite laser generator configuration; third, to address the problem of spatial noncooperative correlation of multiple electromechanical devices in the system, the unified introduction of monocular vision measurement technology completes the external environment information cognition and feature measurement; research eye-in-hand and eye-to-hand monocular measurement configuration under the image capture-analysis-processing-understanding-output technology. For the interconnection of hardware and software of the integrated system of processing and inspection and the realization of equipment cooperation, we compile the processing and inspection process control configuration software based on human-computer interaction graphical interface.

2. Current Status of Research

With the rapid development of industrial robotic arm technology, industrial robotic arm operation tasks are becoming more and more complex, and thus, its spatial positioning, motion guidance, trajectory planning, and task feedback are increasingly dependent on the support of measurement sensors; sensing information gives the robotic arm closed control system external environment analysis and perception capabilities, so that the robotic arm can independently adapt to complex dynamic working conditions, intelligent and efficient to complete the target task [6]. Compared with traditional tactile sensors, vision measurement sensors are noncontact measurement devices, both to avoid the collapse of the object to be measured damage and both information-

rich, easy to analyze characteristics. In recent years, machine vision and its image processing and analysis technology have been applied to industrial robotic arm servo control processes in large numbers, which improves the flexibility and accuracy of the motion system and has an irreplaceable role [7]. According to different classification criteria, the industrial robotic arm of joint machine vision can be divided into a variety of types: according to the number of cameras, divided into monocular vision servo, binocular vision servo, and multivision vision servo system; according to the camera capture station, divided into eye-in-hand and eye-to-hand two categories; and according to the type of control loop-based information, divided into image-based vision servo, based on the position-based vision servo, and hybrid vision servo [8]. Meanwhile, as the target interaction object transforms from static placement to spatial dynamics, higher requirements are put forward for industrial robotic arm grasping, alignment and processing motion planning methods, and control techniques, and the research focus of the joint machine vision industrial robotic arm changes, focusing on dynamic identification and intelligent control. Wu et al. proposed a dynamic gesture recognition method based on optical flow analysis and sequence modulation to control the humanoid robot arm motion through training and recognition of feature images to achieve intelligent control of end motion [9]. Nordal and El-Thalji proposed a dynamic sorting technique for the industrial robotic arm, which automatically acquires the characteristics of the operation object and classifies them based on the image sequence, maintains the sorting target traces, transforms the object coordinates based on the advance compensation, and realizes the sorting action [10]. Haghi et al. proposed a dynamic control algorithm for industrial robotic arm based on active structured light image feature point tracking, which achieves strong reflection interference control based on the integrated application of template matching and feature point association [11]. The algorithm is based on the integrated application of template matching and feature point association to achieve real-time tracking of cutting points under the condition of strong reflection interference.

Fiber optic grating sensor as a better performance sensor is regarded as the future direction of sensor development in the field of mechanical equipment monitoring [12]. Fiber optic strain sensor has many advantages such as small size, high accuracy, no electromagnetic interference, and corrosion resistance. It can measure dynamic strain with faster change and has better stability compared with the vibrating string strain sensor. The current vision sensor technology has been very widely used in industry, science, and technology, and other fields are widely used. Among them, industrial inspection, medical image analysis, traffic safety, home appliances, and other fields of application are more typical. And fiber optic technology has good application prospects in displacement measurement, cable force measurement, temperature measurement, etc., which is very suitable for health monitoring of large machinery and equipment [13]. Fiber optic grating sensors in the major machinery and equipment health monitoring system cannot replace other kinds of sensors because the installation requires many auxiliary facilities, and the field deployment controls difficulties and high cost, but because of the inherent advantages of fiber optic materials, fiber optic grating sensor still has great prospects for application [14]. The overall response of the structure includes structural vibration, displacement, deformation, and turning angle, all types of bridge types should be monitored for vibration and deformation, and displacement and turning angle can be determined according to the selection of structural force characteristics. The vibration sensor is an important part of the sensor subsystem, and the collected data can be used to analyze the change of the structure's inherent frequency to do further damage identification. There are more types of vibration sensors, including capacitive acceleration sensors, servo acceleration sensors, force balance acceleration sensors, and fiber optic vibration sensors. Due to the low self-oscillation frequency of mechanical equipment, the vibration sensor should be selected in the selection of mechanical equipment vibration sensor with a low lower limit of the frequency band, wide frequency band, and large dynamic range. Displacement monitoring includes main beam deflection, bridge pier settlement, and bridge tower displacement.

The predecessor of structural health monitoring is structural inspection based on manual inspection. With the development of science and technology and the rapid progress of network communication, data transmission, and sensing technology, there is a sufficient technical basis for the construction of intelligent monitoring systems. Mechanical equipment health monitoring is not a simple improvement of the traditional detection technology, but a comprehensive use of modern advanced nondestructive sensing technology as well as communication technology, all-weather monitoring of the structural response of mechanical equipment under natural environmental excitation, to obtain all kinds of monitoring information reflecting the state of each part of the structure and the environmental load, and through monitoring, information to analyze whether the structural characteristics have changed, to assess the safe operation of mechanical equipment reliability of mechanical equipment, the evaluation results as a reference for the later mechanical equipment management and maintenance decisions to provide a scientific basis.

3. Performance Analysis of Vibration Sensors for Closed-Loop Feedback Health Monitoring of Mechanical Equipment

3.1. Design of Closed-Loop Feedback Vibration Sensor System for Mechanical Equipment. Mechanical equipment health monitoring system is integrated by hardware and software parts together, mainly to realize the intelligence and real-time of the monitoring system to ensure to get long-term stable and reliable monitoring data, through the daily operation of mechanical equipment structure response all-weather monitoring, accurate access to mechanical equipment status information analysis of change trends, and safety assessment of mechanical equipment [15]. Vibration sensors are classified according to the mechanical quantities

measured: displacement sensors, velocity sensors, acceleration sensors, force sensors, strain sensors, torsional vibration sensors, and torque sensors. Vibration sensors can be used for long-term monitoring of vibration and displacement in machinery, thermal expansion of rotor, and housing; online automatic detection and automatic control of production lines; and measurement of many kinds of tiny distances and tiny movements in scientific research, etc. The health monitoring system should first realize the main functions of the system, and according to the structural characteristics, the monitoring items required for different functions are not the same. The design of monitoring content and the selection of instruments and equipment should consider the characteristics of structural mechanical properties and natural environmental factors. The health monitoring system should first realize the main functions of the system, and the monitoring items required for different functions are different according to the structural characteristics. The design of monitoring content and the selection of instruments and equipment should consider the structural mechanical performance characteristics and natural environmental factors [16]. The health monitoring system is a real-time monitoring system with long service life, and the service life of the monitoring system and the durability of each hardware part should be considered at the beginning of the design, as well as the reliability of the monitoring data and the reliability of the analysis method. The key part optimization refers to the vulnerable elements, deformation sensitive areas, or key parts of the structure due to the structural characteristics, and such areas must be monitored in a focused manner. At the same time, the overall performance monitoring of the structure should also be considered, such as the dynamic performance monitoring of mechanical equipment. Based on the above principles, the mechanical equipment health monitoring system is a set of hardware-based facilities, professional software as the platform and the hub, and hardware and software combined with the automated monitoring system, where the hardware facilities can be divided into three modules, respectively, sensors, data acquisition, and transmission equipment, data management server, and its structure relationship is shown in Figure 1.

The performance of the sensor determines the reliability of the monitoring data, but also directly related to the whole mechanical equipment health monitoring system is good or bad, and the selection of sensors should follow the following principles. The general technical characteristics of the sensor should meet the measurement requirements, and the general technical characteristics mainly include range, sensitivity, resolution, and size. The sensor should have good durability and anti-interference to ensure that it is stable and reliable during its service life. The data acquisition method between the sensors of each monitoring project can collect multiple monitoring contents using the same collection box due to the existence of certain compatibility. The arrangement of sensor measurement points plays a key role in the structural health monitoring of machinery and equipment, and the advantages and disadvantages of the arrangement of measurement points are not only related to the economic cost of the health monitoring system but also related to whether the design purpose of the monitoring system can be achieved. Theoretically, the more sensor points are arranged, the more comprehensive the structural monitoring information obtained, and it is especially important to arrange the sensors reasonably to consider the economy. The following requirements should be met when arranging the measurement points: The actual engineering structure has many degrees of freedom, and it is neither practical nor economical to monitor deformation or stress for all the degrees of freedom. Therefore, the location of the sensors should reflect the principle of optimization, using as few monitoring sensors as possible to obtain the most reliable and detailed structural response of mechanical equipment in operation. The locations of the measurement points must be representative and reflect the maximum strain and deflection of the structure. The performance of the hardware acquisition equipment should be sufficient for the sensors and should have a certain amount of redundancy, reserving a certain amount of performance reserves to ensure the reliability of the system or to meet the needs of future improvement, expansion, and system upgrade. Health monitoring system is based on sensor network technology and based on wearable computing through wired (or wireless) networks for real-time collection and multilayer fusion of contextual information on human physiology, activity, location, and environment, and local or remote processing of this information to make diagnosis or prediction of the user's current or future physical condition. It can provide low-load, noninvasive, and long-term continuous physiological monitoring for patients, realize timely communication and real-time contact among patients, hospitals, and family members, as well as information exchange and convenient consultation between hospitals so that medical health monitoring can realize information access and sharing, and significantly improve medical services. The installation process of various types of sensors and supporting acquisition equipment at the project site should not conflict with each other, and the sensor deployment process should not cause major damage to the structure.

Resonant sensor resonator in a specific test environment outputs a stable resonant frequency signal, and when the measured change, the resonant frequency changes, and the change in resonant frequency can reflect the change in the measured parameters. Resonant sensor structure has a string type, vibration cylinder type, vibration beam type, vibration membrane type, and piezoelectric type, and its advantage is that the output frequency signal can be easily converted into a digital signal, for the subsequent single-chip or computer system to identify the processing; frequency signal can also be modulated demodulation technology for long-distance transmission or detection with little distortion and long-distance transmission signal, although the amplitude of weakening but the frequency characteristics remain unchanged [17]. The resonator has a simple mechanical structure, stable performance, long service life, high-quality factor, low energy required to maintain the vibration state, low power consumption, and low drift. The research in this paper is about beam structure resonators, which can be classified as a single-ended fixed cantilever beam, double-ended,

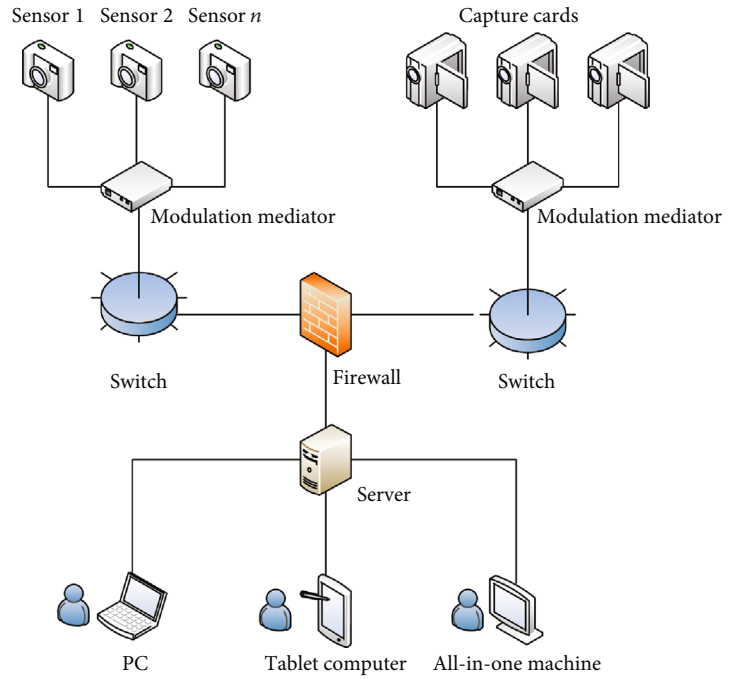

Figure 1: Hardware architecture of health monitoring system.

and four-sided fixed according to the number of constraints. Taking the gas sensor as an example, the thickness direction of the gas sensor is superimposed by different materials with different expansion coefficients, and it is easier to release the internal stress caused by the temperature action by choosing the cantilever beam structure. Under the action of the same excitation voltage, the amplitude of the cantilever beam is larger and easy to detect, so the sensor studied in this paper is a cantilever beam structure.

When the resonant gas sensor is placed in a special gas environment, the adsorption rate of the sensitive layer to the gas molecules is greater than the desorption rate, the equivalent mass of the resonant beam increases, and the resonant frequency decreases; when the sensor leaves the gas environment, the desorption rate of the sensitive layer to the gas molecules is greater than the adsorption rate, the equivalent mass of the beam decreases, and the resonant frequency increases. The resonant beam of the resonant gas sensor has a tiny mass, and its equivalent mass can be changed rapidly when the gas molecules are rapidly adsorbed and desorbed, thus obtaining high sensitivity and response speed. Compared with conventional gas sensors using a gas resistor as the core element, resonant gas sensors are characterized by rapid response, high interference immunity, long life, and high resolution.

$$\begin{cases} J_i = \dfrac{I_i a}{S^i}, \\ J_j = \dfrac{I_j a}{S^j}, \end{cases} \tag{1}$$

$$J = \frac{I_1 aY + I_2 bY}{(X - Y)S}. \tag{2}$$

For gas sensors, the gas to be measured is adsorbed in the sensitive layer by chemical interaction to cause the resonator mass change, so the gas sensor increases the influence of the chemical field than the pressure sensor, and the working environment is more complicated. To improve the sensitivity of the gas sensor to the resonator mass change, the resonator is selected as a cantilever beam structure. In this chapter, the model of the nonlinear dynamics of the cantilever beam gas sensor under the action of multifield forces is established, and the effects of molecular force nonlinearity, gas damping force nonlinearity, and electric field force nonlinearity are considered comprehensively to analyze the multifield coupled nonlinear vibration of the gas sensor.

$$\xi = \frac{p_{ij} A}{p_{ij} - \beta/\alpha(1 + e^{at})we}. \tag{3}$$

For cantilever beam structures, the boundary conditions can be listed for the deflection and angle of rotation of the beam at the fixed end to be equal to zero and the moment and shear of the beam at the free end to be equal to zero.

$$\Delta q = \frac{U_0 E_0^2 d \sin \omega t}{v_v - y}. \tag{4}$$

The coating of the cantilever beam on a gas-sensitive resonant sensor is the key to sensor sensitivity and requires that the adsorption and desorption of the gas are reversible and the process is easy. Plexiglass is a commonly used engineering plastic that can be dissolved in ethanol or acetone and is reversible, so it can be used as a sensitive layer material. Dissolve 1 g of Plexiglas in acetone 50 ml, with the help of a microscope and micropanning table, use the tool to apply

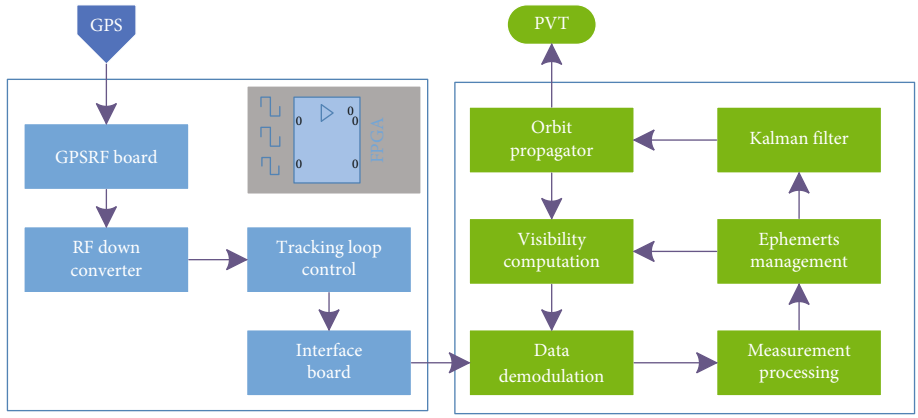

Figure 2: Block diagram of the signal processing module.

the solution evenly on the surface of the cantilever beam, and after the acetone evaporates, a sensitive film of uniform thickness can be obtained on the surface of the cantilever beam, and the thickness of the sensitive layer is measured as 1.5 μm. When the ratio of Plexiglas to acetone solvent is too large, the solution is sticky and the coating layer is not flat and uniform; when the ratio is too small, the coating once cannot reach the predetermined thickness, and the repeated operation tends to make the coating uneven, as shown in Figure 2.

The oil-motor hydraulic system can be divided into two operating states, normal regulation, and quick-closing buffer, according to its role in the turbine system. The normal regulation state refers to the process of normal adjustment of the steam valve by the oil motor, the core control element is the servo valve, and the actuating element is the hydraulic cylinder of the oil motor. In the linear range of the sensor, the higher the sensitivity of the sensor the better, because only when the sensitivity is high, the value of the output signal corresponding to the measured change is relatively large, which is conducive to signal to process, but it should be noted that the sensitivity of the sensor is high, and the external noise unrelated to the measurement is also easy to mix and will also be amplified by the amplification system, affecting the measurement accuracy; therefore, the sensor itself should have a high signal-to-noise ratio to minimize the introduction of interference signals from outside. The fast-closing buffer state refers to the process of fast-closing the steam valve when the oil motor encounters an emergency, and the oil motor drives the piston of the oil motor hydraulic cylinder to reset under the action of spring force and close the steam valve. This chapter models the oil motor from these two aspects and analyzes its prone fault types through the oil motor Amnesia simulation model, to guide the optimal arrangement of measurement points and sample data selection for fault diagnosis modeling of the oil motor condition monitoring and fault diagnosis system and provide theoretical guidance for data access to the industrial Internet platform.

3.2. Health Monitoring Vibration Sensor Performance Analysis. Given the multisurface homogeneous functional structure of complex thin-walled curved parts, there is an urgent need for a multidegree-of-freedom collaborative machining interaction unit that can provide all-round, multiattitude subtractive tooling, to realize the orientation change of the surface area to be machined in the double-sided or even multisided machining process based on the advantages of the body's flexibility through simple pitching, deflecting, and tumbling movements [18]. However, the existing machining equipment and the corresponding preparation process do not yet have the abovementioned characteristics, and it is difficult to realize the complex process requirements of complex thin-walled curved parts. As a multiaxis drive mechanism widely used in industry, the multidegree-of-freedom tandem industrial robotic arm provides a practical solution for the realization of special processes in complex paths with its high flexibility, high spatial accessibility, and high controllability. Resonators are electronic components that produce resonant frequencies, and commonly used are divided into quartz crystal resonators and ceramic resonators. The role of frequency generation, with the characteristics of stability and good anti-interference performance is widely used in a variety of electronic products. The frequency accuracy of quartz crystal resonators is higher than ceramic resonators, but the cost is also higher than ceramic resonators. Resonators mainly play the role of frequency control; all electronic products involving frequency transmission and reception require resonators. At the same time, the multipulse laser etching technology destroys the physical structure of the target material through laser convergence irradiation based on the high thermal effect of light energy to achieve precise forming processing without macroscopic cutting force, and its characteristics precisely match the requirements of complex thin-walled curved parts with multisurface functional structure forming process, while compensating for the low stiffness of the industrial robotic arm. It is assumed that the combination of multipulse laser etching technology and multidegree of freedom industrial robotic arm can realize the high precision and high efficiency of complex thin-walled curved parts, effectively eliminating many shortcomings of the existing processing technology due to the defects of the processing equipment and significantly improving the processing accuracy and efficiency. Because of this, based on the analysis of the characteristics of the existing machining

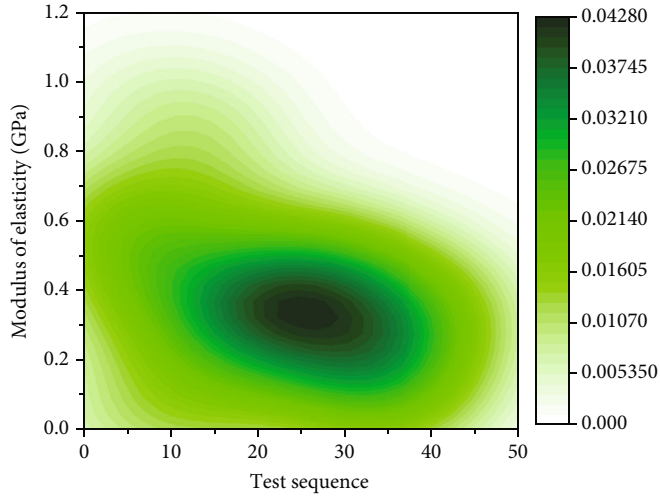

Figure 3: Experimental design values of parameters to be corrected.

equipment and machining process and considering the technical feasibility and implementation cost, this chapter proposes a digital machining method that can realize the single machining of complex thin-walled curved parts and develops a collaborative machining interaction unit with high flexibility, high machining efficiency, and high accuracy, as shown in Figure 3.

The sensitive layer deposition procedure is like 2-8i and requires the arrangement of high-temperature tape on the silicon wafer to cover the noncantilever beam portion of the upper pole plate in Figure 3 to allow for lead pads. After the experiment, the vacuum chamber must be completely cooled before opening to prevent the sensitive layer from oxidation by air. After the pole plate bonding and become a truly independent wafer, itself fragile and vulnerable and no output leads need to be led and encapsulated to protect [19]. The metal encapsulated TO-99 tube of the op-amp is selected as the support base, and the sensor is still fixed to the base with UV adhesive and then led with a WL-2042 ultrasonic aluminum wire crimping machine. The lead wire used in the experiment is a 25 μm diameter high purity aluminum wire. The relative position of the sensor and the tube base should be arranged so that the lead wire spacing is as small as possible to reduce the lead wire impedance and the risk of electromagnetic interference.

The resonator used in this paper works on the principle of electrostatic excitation-capacitance detection, and its structure is equivalent to a flat capacitor, where the upper and lower pole plates are conductive layers, and the insulating layer of the connecting part ensures the electrical isolation of the pole plates. When a DC voltage is applied to the two plates, the mutual attraction of the electric field force between the plates causes the upper plate to bend downward. When an AC excitation is applied, the electric field force between the plates varies periodically, and resonance occurs when the frequency of the excitation force is close to the intrinsic frequency of the cantilever beam, i.e., the strongest output amplitude is obtained at a specific excitation state.

$$i = \frac{d(Cu)}{dt}, \tag{5}$$

$$i_w = \frac{p_{ij} - \beta/\alpha(1 + e^{at})w}{U_0 E_0^2 d \sin wt}. \tag{6}$$

The initial frequency of the phase-locked loop is set to the middle of the predetermined frequency range, the output of the phase-locked loop is a sinusoidal signal, and the feedback signal is processed by a mixer as the excitation signal of the sensor. The excitation signal after the phase shifter is processed by the automatic gain control module AGC to obtain the excitation signal amplitude matching the sensor capacitance and the equivalent capacitance ratio and to meet the stable amplitude condition of the closed-loop system, i.e., the absolute value of the amplitude of the transfer function is greater than 1. The feature of AGC is that the output signal amplitude is automatically adjusted to the set value for any amplitude signal in the range, while the ordinary amplifier is limited by the bandwidth product to amplify at different input frequencies. The amplification is not the same for different input frequencies due to the limitation of the bandwidth product. The equivalent capacitance method is used to offset most of the fundamental frequency components of the sensor, and the mass sensor is placed in a vacuum cavity, and the inverse of the matching capacitance to sensor capacitance ratio is the corresponding AGC output ratio [20]. After I/V conversion, the output signal contains a large amplitude of fundamental frequency components, and the triplet frequency part of the useful signal is weaker than the fundamental frequency signal, so it cannot be extracted directly, and even if the I/V signal is completely extracted, it is still difficult to extract it by filtering algorithms such as wavelet filtering, so a high-frequency filtering module is required. Referring to the lock-in amplifier principle, the multiplier module and the high-frequency filter module are combined to become the inverse lock-in amplifier to realize

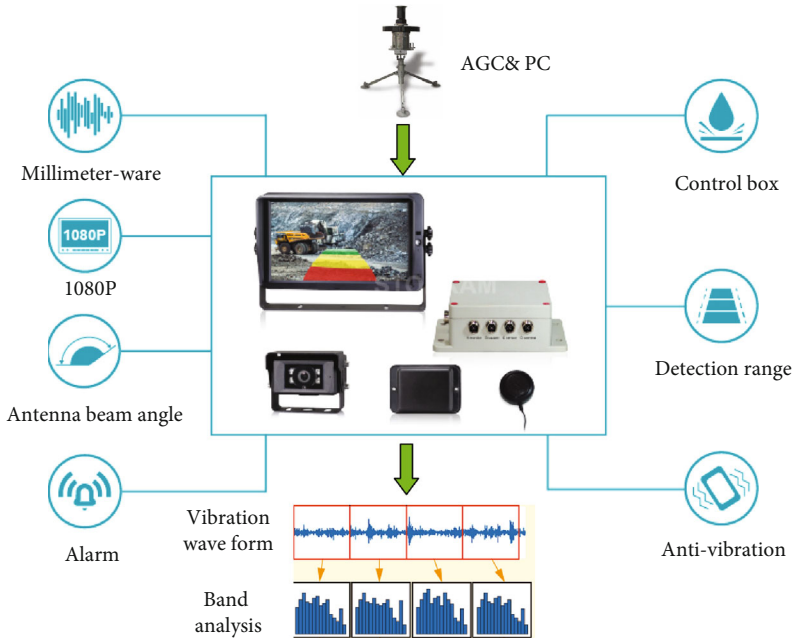

Figure 4: Principle of the high-frequency detection system.

the filtering function for the high-frequency weak signal. The inverse lock-in amplifier migrates the triplet frequency component to the quadruplet frequency, and the reference input of the multiplier is the fundamental frequency component of the lock-in loop output, while the lock-in loop output signal is used as the reference source of the microcontroller, as shown in Figure 4.

During the simulation solution of the virtual prototype model, the chain drive system operates under the driving action of the drive sprocket, and there are complex force relationships between the different components of the system: the scraper and the frictional forces between the scraper chain and the transport chute, etc. Under the combined action of multiple forces, the scraper chain and scrapers can cycle along the transport chute. Therefore, the construction of the virtual prototype model requires comprehensive consideration of the motion characteristics and force features of each component of the chain drive system, and then, the motion constraints and load conditions are reasonably imposed [21]. The constraint relationships between different components of the chain drive system are set, and the constraints between the sprocket and other components are mainly considered for the head and tail sections, where a planar rotating sub is set between the sprocket and the system frame. The contact subsets are set between the sprocket and the cross-chain and between the sprocket and the scraper, respectively. For the body part, the main consideration is the constraint relationship between the transport chute and each component of the single-chain system, where a fixed sub is set between the transport chute and the ground frame. The transport chute and the scraper and the transport chute and the vertical chain are set in contact with each other. The scraper and the horizontal chain in contact with it are fixed. A contacting sub is provided between the adjacent cross-chain and the vertical chain. In addition, the operation of the sprocket can be simulated by applying a rotary drive at the rotary sub of the driving sprocket.

4. Analysis of Results

4.1. Performance Results of Closed-Loop Feedback Vibration Sensor Systems for Mechanical Equipment. The experimentally recorded frequency data curves are shown in Figure 5, the system frequency was 204.46522 MHz when the feedback gain G2 was 300000, and then, the initial position was set again in Section 3.2 after the position of the electric baffle was changed by mistake, and some gold atoms were deposited on the sensor during this process. The weight of the atoms deposited on the end of the sensor is the key parameter in the mass sensor test, and the secondary vertical axis is set as the amount of change in the vibrational mass of the metal atoms deposited by the sensor. The sensitivity of the sensor characterizes the relationship between the amount of frequency change and the amount of mass change, and the sensitivity of the sensor can be calculated by converting the frequency change to the corresponding mass change using the mean value method according to the sensitivity of the sensor.

"Throttle mass" and "root mean square of the throttle" is the experimentally obtained frequency throttle and its root means square according to the sensitivity of the sensor mass characteristics; the throttle mass is the test obtained gas molecular mass, according to the gold atomic standard mass 0.327 zg. Analogy formula (5) can be obtained from the standard mass of H and ethanol molecules, comparing the mass of the knotted mass and the standard mass can be obtained from its error percentage, the percentage of error of ethanol molecules is larger because the frequency stability of the atmospheric pressure state is poor, and the atmospheric pressure state cannot completely exclude the interference

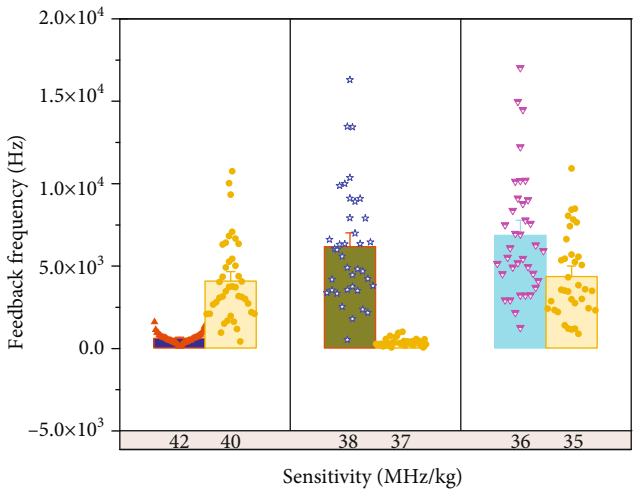

Figure 5: Testing key parameters.

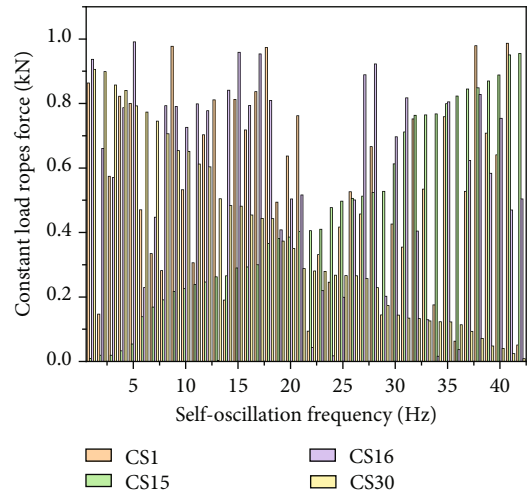

Figure 6: Joint hydrostatic correction results.

of other factors. The knotted mass of H plus the root mean square mass of the knotted mass can be included in the standard mass; the knotted mass of ethanol plus the root mean square mass is very close to the standard mass, indicating the correctness of the experimental results and the frequency characteristics of the nodal difference of the gas test with the mass characteristics; the mesh-filled body in the figure is the theoretical value, the solid-filled body is the measured value, and the line segment indicates the tolerance band of the measured value. Ultrasound has high frequency, short wavelength, and small bypassing phenomenon, especially good directionality, can become a ray and directional propagation and other characteristics. Ultrasound on the liquid, solid penetration ability is very large, especially in the sun opaque solid; it can penetrate the depth of several dozen meters. Ultrasound encounters impurities or interfaces will produce significant reflection to form a reflection into echoes, and ultrasound encounters active objects can produce Doppler effect. In particular, diagnostic ultrasound probes use ultrasound transducers with low power and relatively low operating temperature, which can work for a long time without failure. Ultrasound probes for medical use have a higher temperature and require separate cooling equipment. The corrected parameter values are substituted into the finite element model to obtain the calculated frequency and calculated cable force, as shown in Figure 6; the results show that the corrected frequency error and cable force error have been reduced to some extent; the error of each correction target value is less than 5%, which is closer to the measured value. The correlation between the calculated and measured vibrations of each order of the finite element model is compared, and the MAC values of each order are above 90%, which proves that the correction effect of the response surface method is more accurate, and the corrected finite element model can be further applied to the static-dynamic analysis of the bridge.

To highlight the advantages of the joint hydrostatic model correction method, the finite element model correction of this cable-stayed bridge is performed using the constant load cable force and the self-vibration frequency separately in this paper, and the calculated results are compared with the correction results of the joint hydrostatic force. The comparison results show that the overall error of vibration frequency of the structure is reduced by using the dynamic response alone, but the error of constant load cable force of the cable-stayed bridge increases, and the total error of constant load cable force of the cable-stayed bridge is reduced by using the static response alone, but the frequency error increases significantly. Therefore, the joint hydrostatic correction considers the bridge dynamic error and the hydrostatic error, and the correction content is more comprehensive, and the correction results are more reliable.

4.2. Health Monitoring Vibration Sensor Performance Results. In many machine vision applications, such as robot navigation, augmented reality AR, and photogrammetry, camera pose estimation is a fundamental part of the technology implementation. By constructing a point-to-point mapping relationship between the object plane and the imaging surface, the relative pose between the current industrial camera and the object plane is measured based on the industrial camera imaging model and vision measurement techniques. In conventional camera pose estimation scenarios, although relying on the natural environment imaging features to back-calculate the pose is a common strategy, but because this type of estimation process is extremely dependent on the strong geometric features and strong contrast texture of the external environment, it will make the back-calculation fail in some scenarios and cannot effectively estimate the camera pose, while the invention and introduction of the reference code lead to the original target noncooperative capture measurement to change to cooperative capture measurement, in which the reference code. When the geometric features are known, multiple sets of datums are tiled at specific locations in the external environment, thus explicitly characterizing the current spatial relative pose of the fitted plane. Based on the extraction of the corner points and edges of the reference codes, it is not only possible to accurately inverse the pose of the industrial camera through

the principle of visual measurement, but also to arrange and sequence the reference codes based on their two-dimensional codes to build a map of the external environment features, which is an extremely comprehensive way to recognize the spatial environment in which the mobile robot is located through a single industrial camera, based on the principle of instant localization and map construction.

The strain monitoring data are monitored and warned according to the strain dynamic warning thresholds established above. The strain monitoring project contains a total of two levels of warning thresholds, yellow warning thresholds for bilateral warnings and red warning thresholds for unilateral warnings. Six of the strain measurement points were selected as warning examples. Figure 7 shows the safety warning examples of some of the strain sensors within half a month, and it can be seen from the time course waveform that only a small amount of data from the S-F1 strain sensor exceeded the yellow warning threshold, and no data exceeded the red threshold. From the example effect, the dynamic warning method has good applicability for strain monitoring which is affected by temperature changes and can be used to achieve scientific warnings for strain monitoring.

The deflection warning thresholds established above to achieve real-time monitoring safety warning function of the deflection monitoring project include the lower limit of the yellow warning threshold, the upper limit of the yellow warning threshold, and the upper limit of the red warning threshold. The data of four measurement points of the main span are selected, for example, as shown in Figure 7, the deflection data of the main span takes days as the period and fluctuates up and down periodically under the influence of temperature, no data exceeds the blue warning threshold range during the example time, which is in line with the normal operation statistics, and the data of the upstream and downstream measurement points of the same section are similar, indicating that the bridge has good stability in the cross-bridge direction. The bridge safety early warning system was established, and the bridge monitoring early warning method was set up for each monitoring item, and two levels of safety limits were established for the yellow warning threshold and red warning threshold. According to the strong correlation between strain monitoring data and temperature, the dynamic warning threshold of strain monitoring was established, and the EMD method was used to strip the temperature strain, fit the linear relationship between temperature strain and measurement point temperature, predict the data by fitting the formula instead of the statistical sample mean, and combine with the statistical standard deviation of live load strain to get the yellow dynamic warning threshold of strain. Statistical analysis of the yellow warning thresholds for each monitoring item is shown in Figure 8.

According to the established secondary warning thresholds, the recent monitoring data of the bridge is used as an example of safety warning, and the monitoring time course of some measurement points for half a month is shown; according to the time course graph, only a few measurement

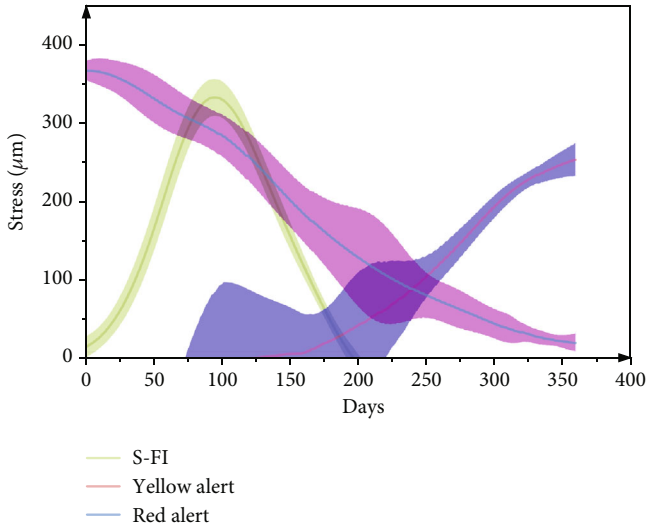

Figure 7: Time-course diagram of early warning for some strain measurement points.

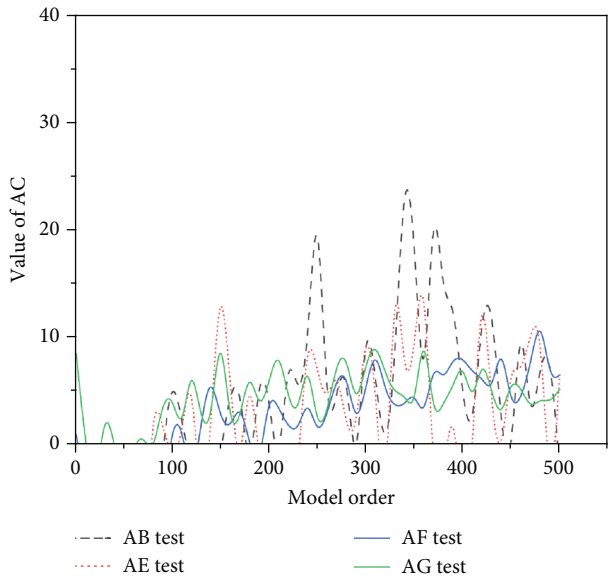

Figure 8: Measured acceleration data AIC fixed-order plot.

points have monitoring data exceeding the yellow warning threshold, and they quickly return to normal, and no monitoring data exceed the red warning threshold. According to the graphs, only a few points exceeded the yellow warning threshold and recovered quickly.

For both sensors, the choice of each influencing parameter can trigger chaotic vibration of the system, which can seriously affect the sensor performance. The chaotic vibration of both sensors can be effectively controlled by the proportional differential control method, among which the chaotic control effect is better for the gas sensor, and the chaotic vibration of each influencing factor can be adjusted to a stable single-cycle vibration, while the pressure sensor is more difficult to achieve single-cycle vibration. The

fourth-order Longacurta method is used to numerically solve the multifield coupled forced vibration theory of the gas sensor resonant oscillator, obtain the chaotic vibration correlation curve of the sensor, determine the stability interval of each influencing factor in the initial stage of the sensor, and verify that the sensor system moves from periodic vibration to chaotic vibration in a doubly periodic bifurcation manner. The influencing factors of the chaotic vibration of the sensor in the gas detection process are analyzed. The chaotic vibration caused by each influencing factor of the sensor is controlled by using the proportional differential control method. It is shown that the chaotic vibration of the sensor can be caused when the parameters are not selected properly. When the initial stage of the sensor is stable periodic vibration, it may also change to chaotic vibration during the test. The chaotic vibration state of the sensor can be effectively controlled by adjusting the control signal gain.

5. Conclusion

The fourth-order Longacurta method is solved numerically for the multifield coupled forced vibration theory of gas sensor resonators, the chaotic vibration correlation curve of the sensor is obtained, the stability interval of each influencing factor in the initial stage of the sensor is determined, and the sensor system is verified to move from periodic vibration to chaotic vibration in a doubly periodic bifurcation manner. The influencing factors of the chaotic vibration of the sensor in the gas detection process are analyzed. The chaotic vibration caused by each influencing factor of the sensor is controlled by using the proportional differential control method. Chaotic vibration of the sensor can be caused when each parameter is not selected appropriately. When the initial stage of the sensor is stable periodic vibration, it may also change to chaotic vibration during the test. The chaotic vibration state of the sensor can be effectively controlled by adjusting the control signal gain. There is a certain error between the calculated structural response and the measured structural response, so the third-order response surface is used to correct the model. The correction results are closer to the actual structural response than the dynamic correction alone or the static correction alone.

Data Availability

The data used to support the findings of this study are available from the corresponding author upon request.

Conflicts of Interest

The authors declare that they have no known competing financial interests or personal relationships that could have appeared to influence the work reported in this paper.

Acknowledgments

This study was supported by the Science and Technology Project of Education Department of Jiangxi, China (Grant No. GJJ151121), the National Natural Science Foundation of China (Grant Nos. 52165015 and 51565037), and the Natural Science Foundation of Jiangxi Province (Grant No. 20181BAB206022).

References

[1] F. J. Mercado Rivera and A. J. Rojas Arciniegas, "Additive manufacturing methods: techniques, materials, and closed-loop control applications," *The International Journal of Advanced Manufacturing Technology*, vol. 109, no. 1-2, pp. 17–31, 2020.

[2] P. Schörghofer, F. Pauker, N. Leder, J. Mangler, C. Ramsauer, and F. Bleicher, "Using sensory tool holder data for optimizing production processes," *Journal of Machine Engineering*, vol. 19, no. 3, pp. 44–56, 2019.

[3] R. Goldoni, Y. Ozkan-Aydin, Y. S. Kim et al., "Stretchable nanocomposite sensors, nanomembrane interconnectors, and wireless electronics toward feedback–loop control of a soft earthworm robot," *ACS Applied Materials & Interfaces*, vol. 12, no. 39, pp. 43388–43397, 2020.

[4] X. Tong, Q. Liu, S. Pi, and Y. Xiao, "Real-time machining data application and service based on IMT digital twin," *Journal of Intelligent Manufacturing*, vol. 31, no. 5, pp. 1113–1132, 2020.

[5] C. Wang, C. Pan, and Z. Wang, "Electronic skin for closed-loop systems," *ACS Nano*, vol. 13, no. 11, pp. 12287–12293, 2019.

[6] Z. Zhu, D. W. H. Ng, H. S. Park, and M. C. McAlpine, "3D-printed multifunctional materials enabled by artificial-intelligence- assisted fabrication technologies," *Nature Reviews Materials*, vol. 6, no. 1, pp. 27–47, 2021.

[7] P. A. Lindahl, D. H. Green, G. Bredariol, A. Aboulian, J. S. Donnal, and S. B. Leeb, "Shipboard fault detection through nonintrusive load monitoring: a case study," *IEEE Sensors Journal*, vol. 18, no. 21, pp. 8986–8995, 2018.

[8] H. Ding, R. X. Gao, A. J. Isaksson, R. G. Landers, T. Parisini, and Y. Yuan, "State of AI-based monitoring in smart manufacturing and introduction to focused section," *IEEE/ASME Transactions on Mechatronics*, vol. 25, no. 5, pp. 2143–2154, 2020.

[9] D. Wu, H. Chen, Y. Huang, and S. Chen, "Online monitoring and model-free adaptive control of weld penetration in VPPAW based on extreme learning machine," *IEEE Transactions on Industrial Informatics*, vol. 15, no. 5, pp. 2732–2740, 2018.

[10] H. Nordal and I. el-Thalji, "Modeling a predictive maintenance management architecture to meet industry 4.0 requirements: a case study," *Systems Engineering*, vol. 24, no. 1, pp. 34–50, 2021.

[11] M. Haghi, K. Thurow, and R. Stoll, "Wearable devices in medical internet of things: scientific research and commercially available devices," *Healthcare Informatics Research*, vol. 23, no. 1, pp. 4–15, 2017.

[12] Z. Li, Y. Wang, and K. S. Wang, "Intelligent predictive maintenance for fault diagnosis and prognosis in machine centers: industry 4.0 scenario," *Advances in Manufacturing*, vol. 5, no. 4, pp. 377–387, 2017.

[13] H. R. Patel and V. A. Shah, "Fault detection and diagnosis methods in power generation plants-the Indian power generation sector perspective: an introductory review," *PDPU Journal of Energy and Management*, vol. 2, no. 2, pp. 31–49, 2018.

[14] Y. Raptodimos and I. Lazakis, "Application of NARX neural network for predicting marine engine performance parameters," *Ships and Offshore Structures*, vol. 15, no. 4, pp. 443–452, 2020.

[15] W. Ahsan, W. Yi, Z. Qin, Y. Liu, and A. Nallanathan, "Resource allocation in uplink NOMA-IoT networks: a reinforcement-learning approach," *IEEE Transactions on Wireless Communications*, vol. 20, no. 8, pp. 5083–5098, 2021.

[16] Q. Mao, F. Hu, and Q. Hao, "Deep learning for intelligent wireless networks: a comprehensive survey," *IEEE Communications Surveys & Tutorials*, vol. 20, no. 4, pp. 2595–2621, 2018.

[17] G. Zhu, D. Liu, Y. Du, C. You, J. Zhang, and K. Huang, "Toward an intelligent edge: wireless communication meets machine learning," *IEEE Communications Magazine*, vol. 58, no. 1, pp. 19–25, 2020.

[18] M. Yan, G. Feng, J. Zhou, Y. Sun, and Y. C. Liang, "Intelligent resource scheduling for 5G radio access network slicing," *IEEE Transactions on Vehicular Technology*, vol. 68, no. 8, pp. 7691–7703, 2019.

[19] S. Yu, X. Chen, L. Yang, D. Wu, M. Bennis, and J. Zhang, "Intelligent edge: leveraging deep imitation learning for mobile edge computation offloading," *IEEE Wireless Communications*, vol. 27, no. 1, pp. 92–99, 2020.

[20] N. Kato, Z. M. Fadlullah, F. Tang et al., "Optimizing space-air-ground integrated networks by artificial intelligence," *IEEE Wireless Communications*, vol. 26, no. 4, pp. 140–147, 2019.

[21] F. Tang, B. Mao, Z. M. Fadlullah et al., "On removing routing protocol from future wireless networks: a real-time deep learning approach for intelligent traffic control," *IEEE Wireless Communications*, vol. 25, no. 1, pp. 154–160, 2017.